Prediction of Olivine Composition Under Limited Calibration Inputs: Comparative Study of Mid-Infrared Reflection, Raman Scattering, and Laser-Induced Plasma Spectroscopies

Sergey G. Pavlov 1 , Iris Weber 2 , Ute Böttger 1 , Ulrich Schade3 , and Jörg Fritz 4,

[1] *Institute of Optical Sensor Systems, German Aerospace Center (DLR),Berlin, Germany*

[2] *Institut für Planetologie, Universität Münster, Münster, Germany*

[3] *Helmholtz-Zentrum Berlin für Materialien und Energie GmbH, Berlin,Germany*

[4] *Zentrum für Rieskrater und Impaktforschung, Nördlingen, Germany*

[5] *Saalbau Weltraum Projekt, Heppenheim, Germany*

Corresponding Author:

Sergey G. Pavlov, Institute of Optical Sensor Systems, German Aerospace Center (DLR), Berlin, Germany. Email: Sergeij.Pavlov@dlr.de

Keywords

Infrared spectroscopy, IR spectroscopy, Raman scattering spectroscopy, laser-induced breakdown spectroscopy, LIBS, vibrational spectra, olivine, space missions, in situ spectroscopy.

Introduction

Analytical optical spectroscopy increases scientific return on missions equipped with landers that accommodate in situ analysis instruments. Robotic extensions of landers such as masts, arms, mini-rovers, and even small drones, greatly increase exploration areas and make instruments, using a sole optical contact for chemical examination of celestial surface materials, the cutting edge of on-board in situ analytics.

To ensure significant scientific return with minimal weight and energy consumption budgets, analytical instruments must have increased capability, accuracy, and depth of analysis even with limited measurement inputs, including on-board calibration targets. In-situ calibration improves the accuracy of spectroscopic data obtained by optical spectrometers, which can be affected by local measurement conditions and accrued instrument alteration. Calibration targets, see Manrique et al., 1 also serve key goals of space missions, providing testing of instrument performance and, in certain cases, monitoring in situ detected changes in parameters of local environments. On the other hand, strict requirements for the size and mass of space instruments imply a very limited set of calibration targets, which at the same time must provide reasonable accuracy. Typically, one mineral per group of the most common rock-forming minerals

(various silicates, calcite, etc.) is selected as a calibration target for in situ measurement. Many robotic missions to distant celestial bodies, often with vanishing gravity, such as asteroids and moons, are designed to run for a short time and only in a few locations, e.g., Kawakatsu et al.; 2 these limitations increase the impact of the quantity and quality of each individual in situ spectrum.

In this paper, we evaluate three main optical analytical techniques used for in situ mineralogical analysis: mid-infrared (MIR) reflectance, Raman scattering, and laser-

induced plasma spectroscopies, for predicting the chemical composition of natural olivine (Ol), (Mg, Fe) $2SiO_4$, with an "extraterrestrial-like" composition, when two natural bulk Ol samples, close to the endmembers of the mineral group, are used as calibration targets. Olivine is a major com ponent in the interiors of rocky planets, i.e., found on the Moon 3 and Mars, 4 is detected in the planetesimal belt, i.e., the proto-Kuiper belt, 5 and is found in samples returned from an asteroid (25,143 Itokawa), 6 a comet (81p/Wild 2), 7 and meteorites. Being an ideal metric of the interior conditions of the environment in which inland minerals were formed, olivine provides insights into the composition of primary melts and their mantle sources. 8 As a rule, higher temperatures during formation yield more magnesium in olivine, while lower temperatures yield more iron. 9 Thus, the composition of olivine, usually expressed in so-called forsterite (Fo) or fayalite (Fa) numbers (we shall use the following definitions Fo# = Mg# = Mg × (Mg + Mn + Fe)−1 × 100 mol%, Fa# = Fe# = Fe × (Mg + Mn + Fe) −1 × 100 mol%) is an important geochemical metric of a local environment. An accuracy of down to about ±1 mol% in olivine Fo# is highly desirable for petrological and geochemical measurements of mantle and igneous ultramafic/mafic rocks. 10 While such accuracy is conventionally achieved by modern laboratory analytics, for example, electron microprobe analyzers (EMPAs), it could be challenging for optical spectroscopies.

The main objectives of this study are: (i) to determine the accuracy of natural olivine composition analyzed by the three main optical spectroscopic techniques used in space missions to celestial bodies with in situ surface analysis instruments, using a limited number of the same calibration targets; (ii) to show that natural olivine end-members in single bulk/crystal form can be used to calibrate MIR reflectance and Raman scattering spectra, using selected published dependences of lattice vibrational frequencies on the composition; (iii) to provide guidance on the use of olivine end-members and the calibrations reported for composition analysis of extraterrestrial olivine.

Solar-reflected infrared (IR) and thermal emission spectrometers, which have long been used for remote sensing, e.g., Bishop et al., 11 have shown great importance for the global survey of the composition of planetary rocky surfaces. The pioneer miniature thermal emission spectrometer on the Opportunity rover has provided mineral abundances and compositions (and other scientific data) at the rover's landing site at

Meridiani Planum, Mars. 12 According to Lane and Christensen, 13 the accuracy of determining the composition of olivine in extraterrestrial regolith can be within ±5 mol% for remote “thermal” IR observation; therefore, even better performance can be expected from a lander instrument. Due to a long heritage and well-developed modeling of IR spectra of minerals, this technique offers a straightforward analysis of IR active vibrational modes in solids without special requirements for samples. However, IR spectroscopy experiences its own challenges in sensitivity and accuracy. It is known that the IR reflectance spectra depend strongly on the sample shape as well as the geometry of the experiment, which should be considered when comparing data and the derived calibrations from different studies. The experimental conditions can range from diffuse reflectance with large hemispherical light collection to specular configurations with small solid angles at different incident angles of the light cone. 14 While the directional hemispherical configurations provide significantly larger intensity and in return are more sensitive to weak spectral features, the bi-directional configurations represent the realistic scenario for remote reflectance measurements at in situ planetary surface studies.

A critical point is the fact that the reflection features of crystal facets of a given mineral naturally depend on the incident angle of light. They do not necessarily occur at predicted wavelengths with well-defined shapes, as is in the case of IR absorption bands. Averaging over the angle of incidence and non-isotropic crystal facets approaches a characteristic spectrum of the mineral. For the space IR spectrometers, a scenario with varying angles of incidence is considered in this study, and averaging the spectra recorded at different incident angles was applied. Bulk targets/crystals with optically polished facets could mitigate the latter challenge by providing MIR reflectance spectra that would depend solely on the defined experimental geometry and not on the surface structure of a calibration target.

Raman light scattering detects frequency-shifted responses of light scattered inelastically by Raman-active vibrational modes of matter. Raman spectroscopy has only recently been considered as an advanced analytical instrument for space probes, e.g., Rull et al., 15 Bhartia et al., 16 and Cho et al. 17 The search for life on celestial bodies by detecting organic matter is one of the main objectives of Raman instruments in the ultraviolet spectral range.16 The space Raman instruments dedicated to geochemical analysis 15,17 are being designed for identification and compositional analysis of rocky surfaces in the visible wavelength range. Raman spectrometers have demonstrated the ability to accurately differentiate mineral phases, which is vital for highly inhomogeneous rocks. The main challenges for Raman scattering lie in low-intense optical responses in the common presence of strong background signals, such as stray light from surrounding sources as well as photoluminescence due to abundant luminophores in rocks. Raman responses also benefit from bulk samples since diffuse scattering from powdered samples significantly reduces the collection of inelastically

scattered light. Since the reported calibrations of olivine rely mainly on absolute values of the Stokes shifts for the two strongest vibrational modes, the accuracy of the calibration can be affected by, for example, a drift of the laser wavelength: this makes an in-situ calibration target of particular importance.

Atomic emission spectroscopy of laser-induced plasmas, also called laser-induced breakdown spectroscopy (LIBS), returns the elemental composition of a target. The analysis utilizes the energy of the emitted transitions as well as their intensities. The latter is proportional to the number of emitting atoms and hence to the ablated molar mass of a single element and can therefore be used for quantitative estimates. An important feature of LIBS analysis is the possible detection of minor and trace elements, which is crucial for many natural rocks. The latter can be used to closely monitor other cations (Ca, Mn) that may be chemically bounded in “compound” olivine (toward Monticellite and Fo + Tephroite types), which can be difficult for other techniques, such as Raman spectroscopy, due to shifts in the weaker vibrational modes. Despite being a relatively robust technique, utilizing intense atomic intracenter transitions, LIBS has inherent limitations in quantitative analysis. These arise from the individual nature of each excited plasma (typically the achieved accuracy is below 5%) and also from the list of elements that can be ionized by multi-photon excitation and/or collisions in the plasma. LIBS has a specific dependence on local parameters, in particular the near-surface pressure, which influences the expansion of the ejected plasma and hence its temperature and the populations of atomic levels.

Laser-induced breakdown spectroscopy (LIBS) was first used on rover missions on Mars 18,19 and recently on the lunar surface. 20 For missions with a limited number of potentially acquired spectra, an in situ calibration of a LIBS instrument would have a large impact. Powdered solid targets typically yield less reproducible plasmas, mainly due to the larger fraction of purely ballistically moving particles/atoms compared to those experiencing the energy transfers (due to collisions and radiation) required to excite electrons and ions in built-up plasmas.

Experimental

Materials and Methods

Samples and Compositions from EMPA. We used two natural olivine samples, with high Mg and low Mg content, representing the “natural endmembers” of the group/solid solution series (see Supplemental Material for more details). The Fo sample (Fo#90.06) is a San Carlos olivine, Fa sample (Fo#1.47) is a Sumatra olivine. The endmembers are large samples (rock slabs) with polished facets of several mm 2. Both samples are highly homogeneous minerals without significant zoning, as shown by EMPA analysis over several points on the surface of the samples, see Table S1(Supplemental Material).

This choice of large bulk samples is motivated by the considerations in the introduction: in order to reduce the influence of sample shape and size.

Terrestrial Fo-rich olivine is the most abundant mineral in the Earth's upper mantle, while Fa-rich olivine is much less common. The higher purity of natural Fo-olivine makes it advantageous as a calibration standard in optical spectroscopy, whereas the greater scatter of vibrational frequencies is inherent for natural Fa samples, which commonly contain more impurities. We selected a troctolite rock sample (common for regolith of celestial bodies without atmosphere, e.g., the Moon, with an olivine composition approximately in the middle of the Fo–Fa line, as the best candidate for evaluating the reported calibrations. The olivine composition of approximately Fo#55 ± 5 was reported from orbital data for a dune field near the area where the Curiosity rover was operating.13 The olivine analyzed is a troctolite (Tr) Figure 1, a part of the igneous rock sample from the Bushveld Igneous Complex, South Africa, with strong zoning, composed of olivine, low-Ca pyroxene, feldspar, and ilmenite Table S1, Supplemental Material.

Spectrometers

We used commercial IR and Raman spectrometers with moderate characteristics spectral resolving power, sensitivity, and suppression of straight light) that are about those used in the relevant space instrumentation. Our LIBS spectrometer has an advanced spectral resolution generally not provided in on-board instruments; however, the results obtained in this study can be extrapolated to the latter due to a large difference in the wavelengths of the atomic transitions used for calibration.

Infrared Microscope

Extended spectral ranges, such as 3–40 μm, which cover almost all IR-active phonon bands of rock-forming minerals, 21 would be highly desirable. However, miniature spectrome ters for space research have severe limitations in the usable components, 22 thus limiting this desired spectral range.

Two MIR ranges: 8–13 μm and 14–28 μm are of great importance because the spectral bands have a large contrast in several spectral regions, which is necessary for in situ studies. The high-frequency range of these two is supported by semiconducting mercury–cadmium–tellurium detectors, which are among space-qualified devices. The ongoing progress in the sensitivity of MIR detectors suggests that the thermal IR spectral range will prove advantageous for in situ mineralogical analysis in future space missions with landers. Mid-infrared (MIR) reflection spectra Figures 2 and 3 were recorded in the range of 5.0–17.2 μm (580–2000 cm^{-1}) with a spectral resolution of 4 cm^{-1} using a Nicolet iN10 IR microscope (see Supplemental Material for more details).

The analytical spot size was adjusted to illuminate most of a single mineral zone and varied between 30 × 30 μm 2 and 150 × 150 μm 2 . Between 16 and 128 so-called single-channel spectra were recorded and averaged. A reflectance spectrum was obtained by normalization of the averaged and reference (a gold film deposited on a polished silicon wafer) spectra. To account for the above-mentioned effects arising from the crystal facets, expected in the samples with strong zoning, at least five measurements for different azimuth angles on a rotating stage of the sample were averaged to form the final spectrum.

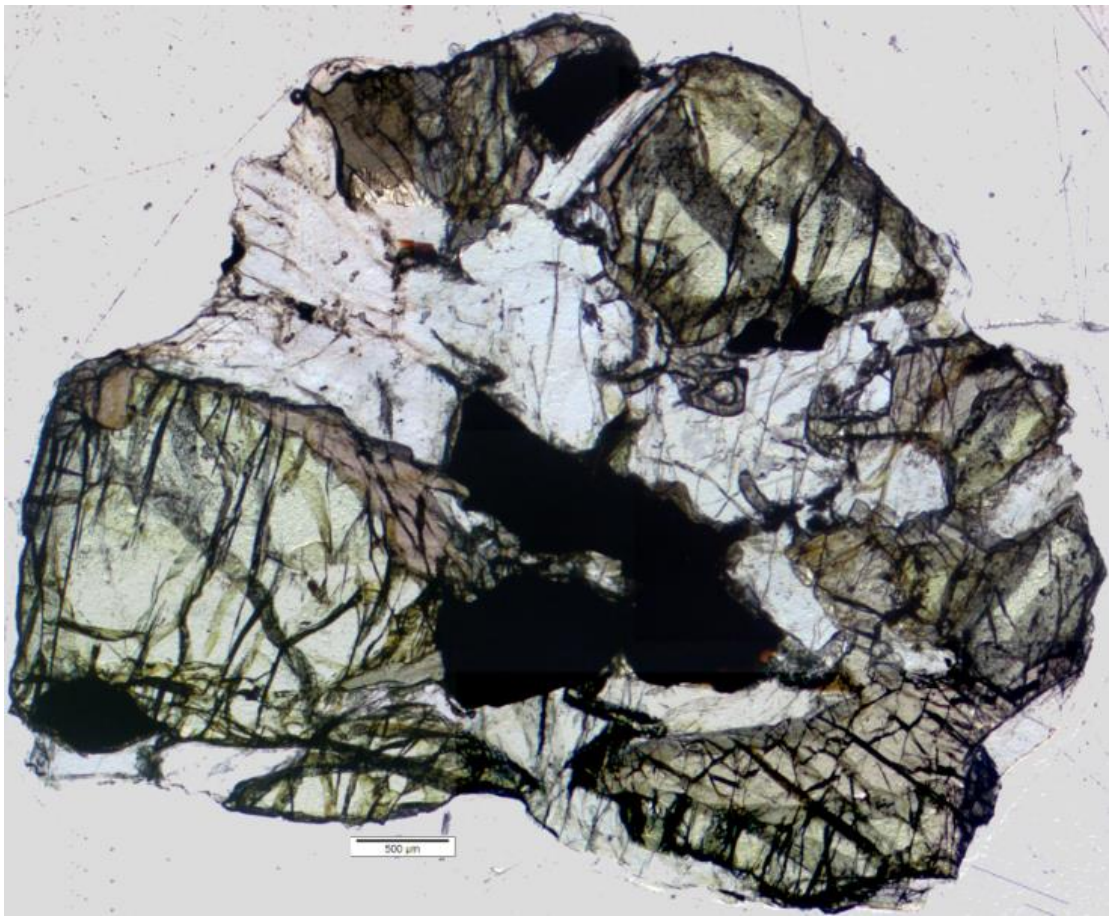

Figure 1. The troctolite sample image by a Keyence digital microscope VHX-500F. The olivine phase is a few mm 2 area (light green) in the left low corner of a sample. The scale segment is 500 μm.

Raman Microscope

The Stokes-shifted light of rock-forming minerals is commonly recorded in the spectral range 200–3700 cm^{-1}. This range can be covered with a device built from pacequalified components with a single semiconducting detector. For example, for a 532 nm laser, often used for Raman spectroscopy of minerals, the required Stokes range spans over 537–662 nm, which is covered by a silicon-based charge-coupled device (CCD) array.

The Raman spectra Figures 4–6 were acquired using a WITec 300 alpha spectrometer (see Supplemental Material for more details) using a 532.2 nm laser. The condensed

beam of ~1.5 µm diameter at the sample with an average power between 1 and 5 mW was used for most of the data used for calibration at the low-intensity end. The spectra were recorded with a series of up to 100 individual spectra and the spectra accumulation time varied between 2 and 30 s. The resolution is 6 cm $^{-1}$ per pixel (spectral resolution: 10 cm^{-1}). The spectrometer was calibrated using the NIST values 23 for the transitions of a Hg lamp in the range of 500–700 nm. The determined dispersion led to the Stokes shift of the longitudinal and transverse optical phonon (firstorder Raman scattering) of the monocrystalline silicon sample (reference) of 520.6 ± 0.2 cm^{-1}. The variations in the wavelength of the neodymium-doped yttrium aluminum garnet (Nd:YAG) laser were compensated by the monitoring in the Rayleigh wavelength (elastic light scattering) for each individual Raman spectrum. We point out that such a procedure is not reported in the publications we cite/used here.

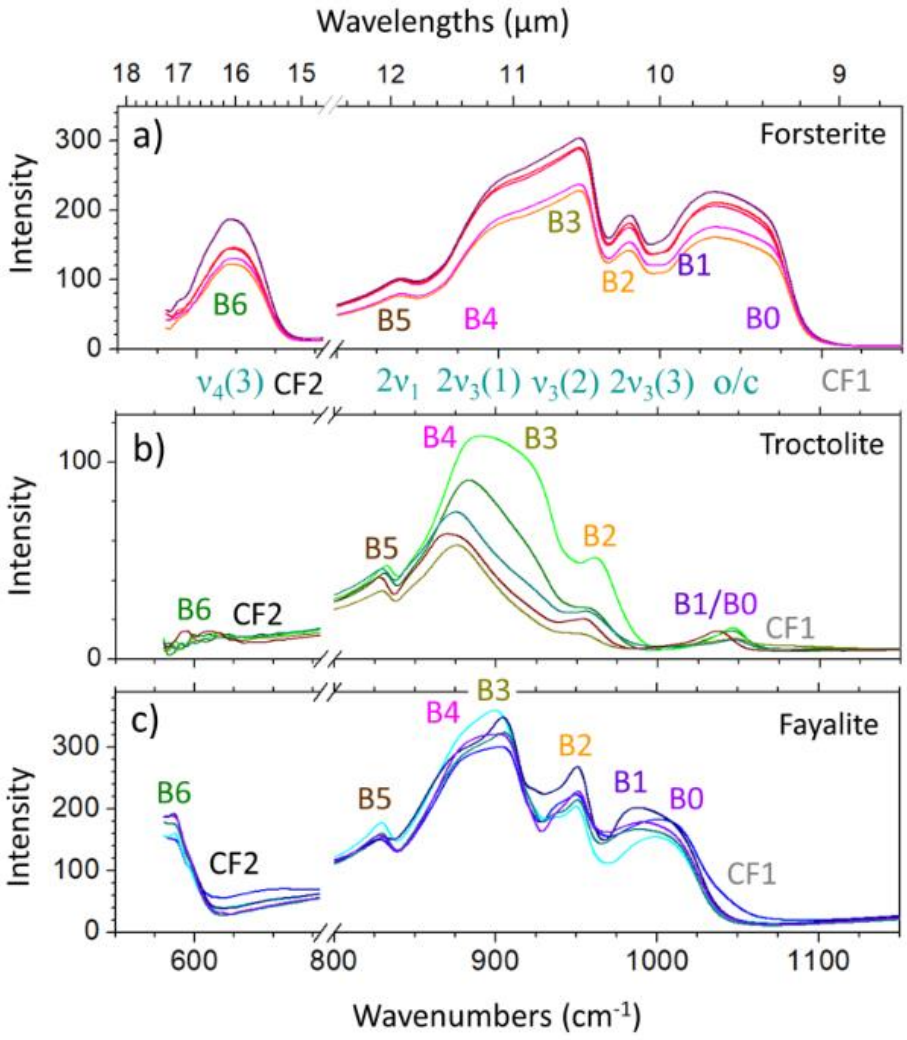

Figure 2. Mid-infrared (MIR) reflection spectra obtained from bulk natural Fo (a), troctolite (b), and Fa (c) samples. Reflection band numbering is B0–B6 27 and the CFs are CF1 and CF2 following Hamilton; 29 Nv m (S) are labels of IR-active molecular vibrations: 26 m = 1 is symmetric Si–O stretching of a SiO 4 tetrahedra; m = 3 are anti-symmetric stretching modes; m = 4 is symmetric bending of SiO4 ; and N are numbers of (here: spectrally unresolved) modes contributing to the bands; o/c stays for vertones/combination phonon bands. Different colors in the plots correspond to different incident angles.

Laser-Induced Breakdown Spectroscopy (LIBS) Spectrometer

Atomic emission spectra of most elements composing silicate minerals can be effectively evaluated by intracenter transitions of neutral atoms in the range 170–820 nm. The spectral range of interest for olivine including its common natural inclusions, can be reduced to 280–780 nm, which is covered by a conventional silicon-based CCD detector. Since these lines occur in groups for each element and extend over a wide range, the requirements for spectral resolution can be relaxed. We used a high-resolution dispersive instrument, but the results can be also extrapolated to spectrometers with lower spectral resolution.

The LIBS spectra Figures 7 and 8 in this study were acquired using an Aryelle Butterfly spectrometer (Laser Technik Berlin; see Supplemental Material), which provides a spectral resolution within 21–52 pm varying over a range of 280–800 nm. Inlite II, a 1064 nm Nd:YAG laser (Continuum), was used to generate plasma from irradiated samples. The focused laser beam spot is ~150 μm at the sample, with a pulse energy of about 20 mJ. The atomic emission spectra were acquired by averaging 50 shot series per site: three different ones on the troctolite sample and four different ones on the reference samples. We hold the sample in an evacuated chamber, at about 100 Pa, to avoid the influence of the ambient atmosphere, which is often absent/dilute on planetary surfaces. Plasmas at higher ambient pressures would generally provide greater brightness for atomic transitions.

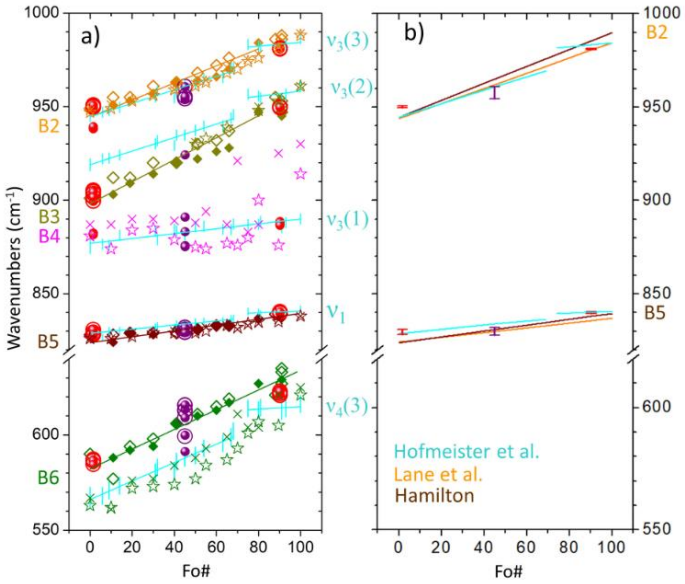

Figure 3. (a) Characteristic IR spectral features of olivine: this study compared with the reported values and IR calibrations. For this study, red/purple open circles are values derived from the original spectra, and closed circles are values from the spectra derivatives. Closed rhombic symbols are data from Clark et al. 33 and open symbols are from Salisbury et al. 21 Stars are peaks obtained from bi-directional reflectance spectra of (crashed Ol) pellets while crosses represent the data from diffuse reflectance spectra of powdered samples.27 Straight lines are the regression fits ν(Fo#) derived in Hamilton; 29 cyan lines crossed by vertical segments are regressions for IR phonon frequencies while the segment size reflects their line widths. Note the different gradients ∂ν/∂x for the ranges Fo#0-69 and Fo#74-100.26 (b) The selected bands with the Fo#(ν) regressions for the reflectivity peaks 26,29 and the stretching phonon frequencies. 26 The vertical line segments (red: calibration Ol samples, purple: troctollite) show the ranges of the frequencies obtained at different incident angles of the diagnostic light.

Results and Discussion

Mid-Infrared (MIR) Reflection Spectroscopy

Numerous studies 24–30 have shown that several features in the MIR reflection spectra, correlated with Reststrahlen bands, can be used to distinguish natural olivine among silicates. These features occur in the MIR part of the wavelength range (8–50 μm; 200–1250 cm^{-1}) and exhibit clear frequency shift trends $\partial v(x)/\partial x$ with varying solid solution composition x (Fe 1−x; Mgx). These high-reflectivity bands comprising IR-active phonons, stretching and bending motions in the silicon–oxygen anions $(SiO_4)^{4-}$ tetrahedra, and also the specific reflection minima due to rapid changes in the refractive index, appeared on the high-frequency side of the stretching bands of silicates, in both reflectance and emissivity spectra, i.e., the so-called the "primary" (CF1) and "secondary" (CF2) Christiansen features (CFs). 27,29 The corresponding bands in the reflectance spectra of natural olivines 27,29 have different regularity to compositions and spectral contrast. While some translational modes exhibit large $\partial v(x)/\partial x$, most of these low-frequency modes were not observed in the reflectance spectra of all-natural olivines. 27,29 The lower frequency modes (referred to as Bands 6–9 in Hamilton 29) have irregularities in the slope with composition and do not serve as good calibration functions. The translational modes (at lowest frequencies, bands up to 12) were not regularly detected in the spectra of all samples. The highfrequency part of this characteristic range (B0–B6: 550–1150 cm^{-1}) comprising stretch and bending modes of the SiO_4 tetrahedra and combinations/overtones 24 and CF1, CF2 are regularly presented in most spectra of olivine with different Fo#, 27,29 and occur to be a reasonable choice for the calibrations of natural olivine in reflectance spectra.

The reflectance spectra measured in this spectral range for our samples, serving as natural "endmember" olivine and troctolite, are shown in Figure 2.

The assignments of the observed spectral features to the vibration modes in the lattice can be taken from absorption spectroscopy 24–26 of the olivine series with various compositions (up to 21 natural and synthetic olivines with Fo# between 0 and 100). The proposed different assignments of the vibrations of anions and cations, including translation, rotation/libration, bending, and stretching modes are shown in Figure 3a. The authors pointed out the excellent agree ment of the frequencies derived by the multi-Lorentzian fit of the absorption spectra to the transversal and longitudinal optical phonon components in the reflectance spectra, 25 as a rule with the uncertainty within full width half-maximum of the bands. The derived gradients of the mode frequency changes with a solid solution, $\partial v(x)/\partial x$, for all spectrally resolved modes Figure 3a, vary from 0.07772 to 0.8346. 26 Remarkably, these data indicate a clear discontinuity in the dependences of phonon frequency on composition v(x) around Fo#70. This is consistent with the observation obtained by Raman spectroscopy in Gaisler and Kolesov. 31

At the same time, most other relevant studies in IR and Raman spectroscopy predict a continuous dependence v(x) described by linear or quadratic regression formulas. This discontinuity could imply the fit accuracy since calibration tudies provide poor statistics for olivine with Fo# > 70 Figure 3a, while the majority of extraterrestrial olivine (for instance ordinary chondrites) fall in this range.32

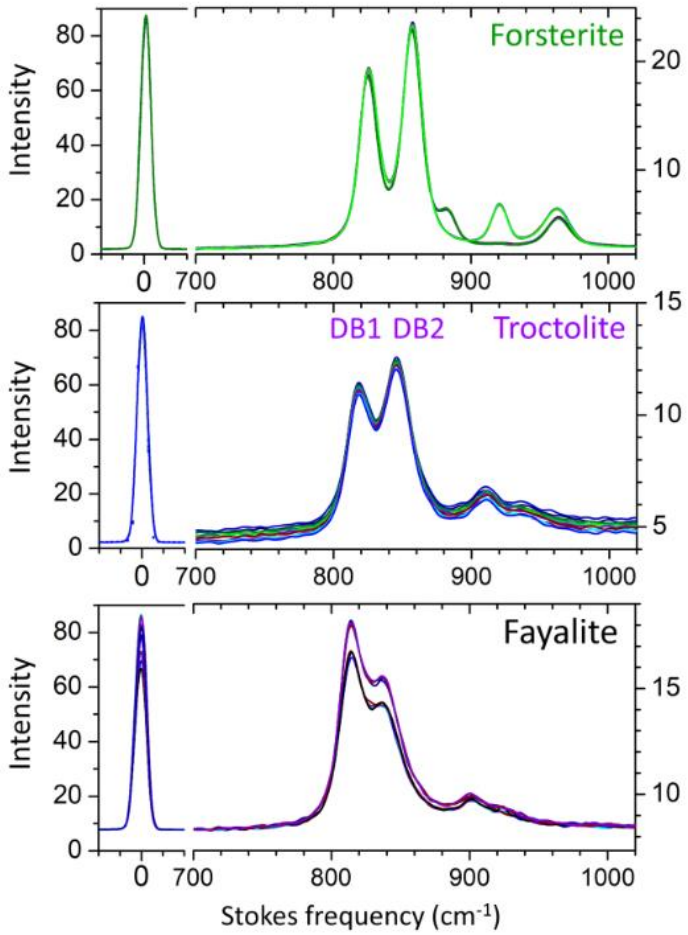

Figure 4. Typical Raman spectra recorded in series (given in different colors) at the selected points of the Ol-endmembers (Fa, Fo) and troctolite (Tr) samples. The left parts show the spectra of the remaining laser Rayleigh scattered light. Note the variations of the Raman signal, which is mainly expressed for the Fa sample, and the variations of the relative intensity of the modes, which occur most strongly for Fo, at different locations on the sample. Note the different scales on the left (for Rayleigh) and right (for Stokes) parts of the plots.

The band's assignment in Lane et al. 27 differs for the broadband 850–940 cm^{-1} comprising 2v3 (1) and v 3(2) anti-symmetric stretching modes, by two spectral features: Bands 3 and 4 instead of the single Band 3 in Hamilton. 29 We shall use this "extended" mode assignment: B0–B6. We determine two sets of reflection band positions in our spectra, which include: (i) global reflection maxima (peaks) in the selected spectral regions covering specific phonon groups and spectrally resolved others; (ii) features in the slopes (presented in the first derivative of the absorption spectra) which includes zeros (i.e., maxima and minima in reflection) as well as points

of large local changes in the slopes (representing, among others, spectrally unresolved local maxima in the broadbands where global maximum is different). The second group introduces additional frequencies, B3/B4 in the spectral region represented by absorption due to 2v 3(1) and v 3(2) phonons (while only one frequency represents the first group for this spectral range) and B0 in the sum phonon band (c/o). The combination modes (B0–B1) at the high frequency end as well as the bending mode B6 appear to be strongly dampened in the troctolite sample, which generally has weaker spectral features. As it is clearly seen (see also Supplemental Material for the determined values of all band positions), all characteristic features in the spectra of our Ol endmembers, the B0–B6 reflection bands, and the CFs, are generally spectrally well resolved and the peak fit well to the reported values.27,29

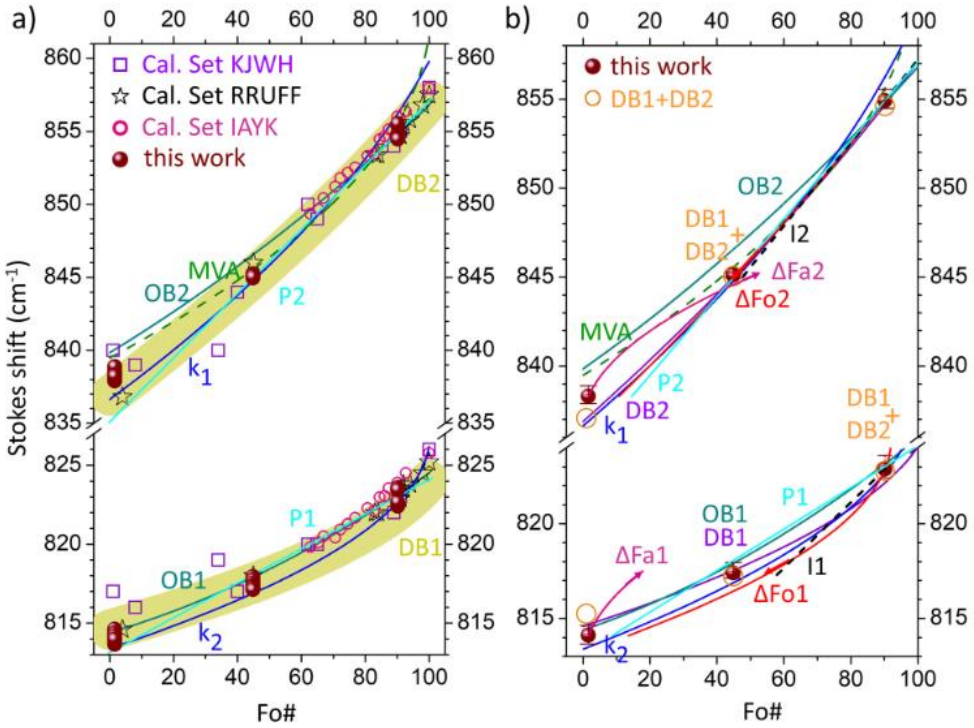

Figure 5. (a) Stokes-shifted frequency of the modes of the measured samples compared with the reported data for olivine sets and with the calibrations of olivines, based on the stretching modes. The broad areas represent "the best fit ellipsoids/main line" for two modes DB1 and DB2 together. 35 The values used in Kuebler et al. 35 calibration set (10 natural, i.e., terrestrial and meteorites, and synthetic olivines) are shown as "Cal. Set KJWH" (squares). Cal. Set RRUFF shows the data set (12 olivines, Fo#4–100) given in do Nascimento-Dias et al. 36 and reported as from the RRUFF database.37 The MVA, performed on the large set (93 natural and synthetic olivines, single crystals, and powdered) of data, is represented by the calibration regression line for the "DB2 centroid" from Breitenfeld et al.38 Calibrations for both bands OB1 and OB2 are the regression models from Torre-Fdez et al.; 39 for both bands k1 and k 2 are the models from Mouri and Enami:40 21 natural and synthetic olivines covering Fo#1–100, monticellite and tephroite. Cal. Set IAYK represents the frequencies of 15 natural and synthetic ("the cores of the grains") olivine covering Fo#62.8–100, from Ishibashi et al. 10 P1 and P2 are the linear regression models from Pittarello et al.41 (b) The mean Stokes frequencies of the measured samples compared with the reported calibrations of olivine based on the stretching modes. DB1 and DB2 are the single-band and DB1 + DB2 is the two-band calibrations from Kuebler et al.35 ΔFa1, ΔFa1, ΔFo1, and ΔFo2 are the quadratic differential, single-band calibrations10 related to the reference samples Fa and Fo and the respective bands. The dashed lines I2 and I1 are linear differential regressions defined for the limited range of Fo#62.8–100 in Ishibashi et al.10

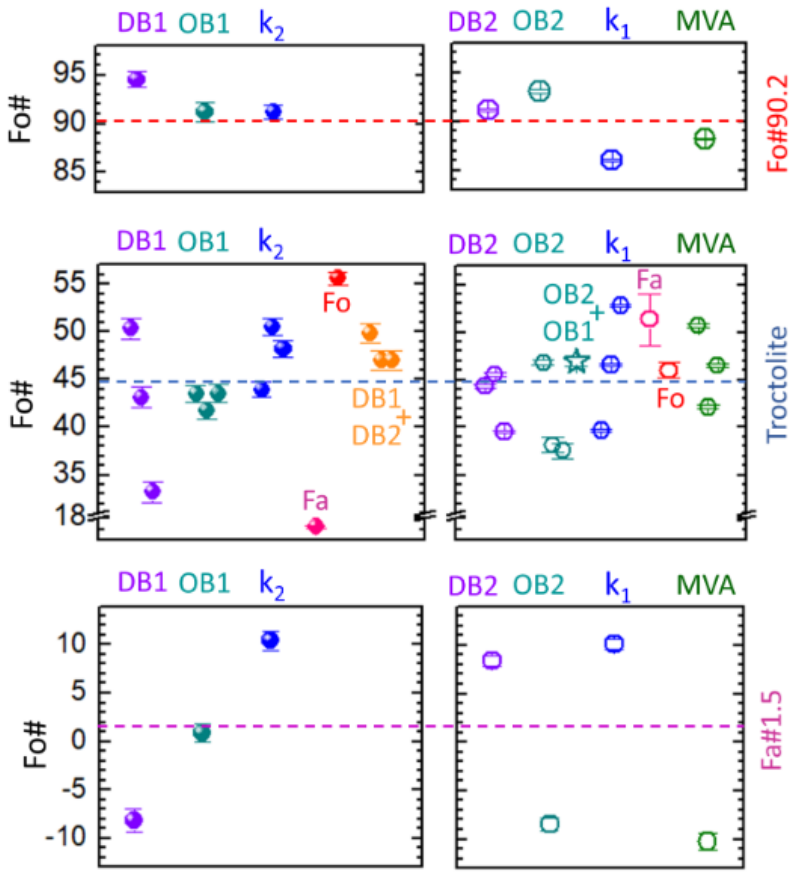

Figure 6. Determination of the Fo# of the troctolite sample (middle) using different regression models. (Top) the models based solely on the high-frequency anti-symmetric stretching band: quadratic regressions on DB2,35 on k1 ,40 from OB2; 39 MVA: multi-variate-based quadratic regression on the "DB2 centroid"; 38 Fa, Fo: using the differential regression on the high-frequency band of the Fa, Fo samples derived in Ishibashi et al., 10 and differential quadratic regression based on two bands (star). 36 (Bottom) The models based solely on the low-frequency anti-symmetric stretching band: quadratic regressions on DB1,35 on k 2, 40 from OB1; 39 Fa, Fo: using the differential regression on the low-frequency band of the Fa, Fo samples derived in Ishibashi et al. 10 DB1 + DB2 shows the set using combined two-frequencies calibration. 35 The dashed line represents the EMPA data for the troctolite sample. In each series of three close points, the middle one is the absolute frequency calibration without using input from the end-members, the left and right points, when the same regression is moved to the Stokes values of the Fa/Fo samples respectively. (Left) One-band calibration results for our Fa sample. (Right) One-band calibration results for our Fo sample.

The mean CF2 frequency in our terrestrial olivine fits well with the reported in Hamilton.29 However, this feature is not clearly distinguishable in all spectra of troctolite, e.g., exhibits two or more minima. Note that only the lower frequency in these split CF2 minima agrees with the regression proposed by Hamilton.29 The main CF in our endmembers is far off the fit proposed in Hamilton,29 while corresponding to the CF1 frequencies of individual olivines obtained from the original spectra in Salisbury et al.,21 the same is true for troctolite. Concluding these observations, the Christiansen features cannot serve as reliable metrics for the accurate calibration of extraterrestrial olivines. The combination band maxima Figure 2 derived from the spectra' derivatives of our natural Ol endmembers fits well with the data in Salisbury et al.,21 while the B0 frequencies are close to the reported IR phonons for Fo and Fa.24,25 They would give a good linear dependence v(x) with the gradients $\partial v/\partial x$ for the c/o Band, close to the B1

linear regression in Salisbury et al.21 and to the specular reflection B1 series in Lane et al.27 However, both sets of spectral features, in the original reflection spectra and their derivatives, migrate strongly in the measurements of our Fa sample at different incident angles of light. Therefore, we exclude the c/o Band also for the Fo#(x) calibration.

The reflection Bands 2–6 represent stretching and bending modes of a $(SiO_4)^-$ tetrahedra, 17 Figures 2 and 3. They have inherent advantages: (i) lesser contribution to the band phonon modes if compared to the CF bands; (ii) offer the use of the complementary asymptotics derived individually from reflection, absorption, and emission spectra.

First, we check where the spectral features of our measured olivines lie on the map v(Fo#) of the reported absolute frequencies in the MIR reflection and absorption Figure 3 using the EMPA data for our samples. Next, we define the IR bands that can be used for calibration. The reflection minima in the IR spectra 29 were obtained on 23 natural olivines (from those nine samples have the same composition) selected from two studies: Salisbury et al. 21 (biconical reflectance spectra of pellets pressed from crashed Ol crystals) and Clark et al. 33 The influence of particle size and specular versus diffuse light collection was studied by Lane et al. 27 for synthetic olivine. The spectral features in the bands were determined from the local “flection position”, defined as spectral minima in 1 − R(v) spectra, over 13 crystals with the crashed/pressed and powdered (particle size <45 μm) samples.

In the cases where the sample was smaller than the light spot at that location, special calibration procedures were applied to reduce the influence of the signal reflected from the sample surroundings. It is clear to see in Figure 3a that the search for band positions in Lane et al. 27 follows the IR phononic bands as in Hofmeister and Pitman, 26 thereby yielding an additional reflection band B4 ($2v_3$ (1)). While these reflection bands generally match better to the phonon absorption spectra, they suffer from some problems: incomplete B3 band and large data scattering for the B4 and B6 bands, more pronounced for the powdered samples.

The peaks for the spectral bands B2, B3, B5, and B6 of the olivine endmembers, obtained from the original spectra Figure 2, are in close proximity Figure 3a to the data from specular reflection of the mixed olivine set in Salisbury et al. 21 Additionally, Band 4 can be used if we add the spectral features obtained from the spectra derivatives Figure 3a, see Supplemental Materials for the tabulated frequency values.

The spectrally resolved and relatively narrow bands representing one or more phonons, such as 2v 1 and v 3(3) phonons, are obviously most useful for asymptotic v(x).

In these particular bands, the peak values from our spectra tend to the lesser gradients and are closer to the phonon frequency values 26 rather than the reflection peak as in

Lane et al. 27 and Hamilton 29 where the discontinuity around Fo#70 is ignored Figure 3.

In our troctolite sample, for the anti-stretching modes (1) and (2), the absolute peak and the second feature seen in the derivative spectrum, reverse their intensity so that the maxima migrate to Band 4, while the weaker derivative features move into Band 3 and are mostly missing Figure 2. The double spectral feature of troctolite in Band 6 represents a specific large incident angle and its low-frequency part can be discarded. Generally, the features in the spectra recorded at these critical angles deviate more from the mean value at each measurement point.

We select Bands B2 and B5 (numbering according to Lane et al. 27) for calibration purposes. From Figure 3b it is clear that our samples do not follow the linear dependence *v*(x) for any spectral band; the Fa sample returns the frequency values with the largest deviations from the reported calibrations on the reflectance features. 27,29 For the selected Bands B2 and B5, the peak values derived from the search in the original spectrum and its derivative almost coincide.

Using the regression formulas in Hamilton 29 for Band 2 and Band 4 (numbering as there) we obtain for the troctolite sample, Fo#44.63 (EMPA): B2, Fo#22–36 (mean 27.28); B4, Fo#26–52 (mean 42.34). Using the regression formulas in Lane and Christensen 13 for Bands 2 and 5, we obtain the troctolite sample: B2, Fo#26–42 (mean 32.20); B5 Fo#28–60 (mean 48.52). When using the mean for the peaks in the spectra of our Ol-endmembers for the calibration of the troctolite sample, we obtain, assuming linear regression v(x): mean values over all spectra: B2, Fo#20.22; B5, Fo#6.93; mean values for the sets excluding the two largest biased values: B2, Fo#31.24; B5, Fo#14.04. The broadening of several vibrational IR-active modes in the troctolite sample shortens the useful spectral range to 800–1100 cm^{-1}. This remains sufficient to distinguish some characteristic spectral features in the MIR range covering stretching and bending modes of the $(SiO_4)^-$ tetrahedra for both (i) differentiation olivines from silicates 28 and for (ii) approximate determination of Fo# using natural olivine end-members as calibration targets. The use of our Ol endmembers does not lead to linear dependences v(x) and thus determines inaccurate values for Fo# of the troctolite sample.

The relatively narrow and well-separated bands are the most suitable for the Fo# calibration of troctolite, using linear regression for *v*1 symmetric Si–O stretch mode, 29 B4: within 5% 27 and B5: within 8%.

When using a linear fit between the natural Ol endmembers in this study, the narrow band B2 (*v*3 antisymmetric Si–O stretch) gives the Fo# ∼30% different from the EMPA data for the troctolite sample. Our Fo and troctolite samples are closest to the linear regression of the B2 band in Hamilton. 29

Raman Spectroscopy

Raman light scattering spectroscopy can address up to 36 Raman-active vibrational modes of olivine. 32 The two strongest Raman lines represent Si–O symmetric, Ag(Si–O) s−str and asymmetric stretching, Ag(Si–O) a−str , vibrational modes in a SiO_4 ion group within the Stokes shift (f) bands within 810–860 cm^{-1}. These bands are well detectable and spectrally resolved (cf. Figure 4) of other modes in the entire range of solid solution composition. The frequency of these modes has been shown to exhibit a quasi-linear dependence on the average cation mass 34,35 yielding Fo#(f) slopes up to 0.2 cm −1 per unit (Fo#), proving to be an excellent choice for Fo# calibration. Although the typical spectral resolution of commonly used grating spectrometers (and also those developed for space missions) is several cm^{-1}, the accuracy of the line peak determination can reach 0.1–0.5 cm^{-1}, and therefore the possible accuracy for determining olivine composition can be expected within several Fo# units. As we discuss here, the uncertainty in Raman spectroscopy arises from the precision of the absolute wavelengths and the spectral dispersion of the instrument over the Stokes-shifted frequency range. This makes calibration targets critical for both the in situ instrument performance and the alteration in material properties. The measured Raman spectra show clear differences in the frequency of the Si–O stretching modes as well as their relative intensities Figure 4. Unlike Fa and troctolite samples, local spectra of the Fo sample exhibit changes in the higher frequency $v_3(B_g)$ modes, $B_{2g}(xz)$ versus $B_{2g}(yz)$, 35 clearly indicating different orientations of some microcrystalline grains in the San Carlos sample.

The derived phonon frequencies v from our spectra fit well into the v(Fo#) map where we collect the reported data from other studies Figure 5a. Laboratory calibrations of olivine composition by Raman spectroscopy have been performed continuously starting from 1996 to the present, using different olivine calibration sets, i.e., mineral origin: natural, synthetic, extraterrestrial, and mixed sets; sample forms: single crystals, crashed, milled to powder; different instruments (in terms of calibrations of the absolute spectral unit, spectral resolution, deposited laser power), and post analysis, i.e., peak search, statistics, and variational analysis.

We address most of these approaches in this work in order to select the best calibration approach for the limited input/number of calibration samples.

We first address the potentially large biases that could appear and strongly affect the calibration at the limited input. Kolesov et al. 42 reported step-like shifts in the Fo# (f) slopes observed in the spectra of 14 natural terrestrial olivines: two steps for A g(Si–O) s−str and one for A g(Si–O) as −str modes, the common one at around Fa#30, that would correspond to the stoichiometric feature at Fo#70 in the MIR spectra as reported in Hofmeister and Pitman. 26 They related this common feature to the predominant occupation of the M1 position in a Fo-like olivine lattice by Fe^{2+} cations. 42 However,

such a step in Fo#(f) could not be detected in later, other studies. Ishibashi et al. 10 determined the linear Fo#(f) slopes using 15 natural terrestrial and synthetic olivines with the small Fo# steps in the range of Fo#62.8–100 using a high-resolution (~1.5 cm^{-1}) Raman spectrometer (see Cal. Set IAYK in Figure 5).

The scatter of the data at low Fo# < 50 Figure 5 is obviously due to both the limited number of available Fa-like olivine samples and the stronger influence of impurities common for natural Fa samples, among others—divalent cations (Mn, Ca, and Ni). We note that the deviations of the low- and high-frequency modes from the Fa "mean" for our Fa-end-member sample, having about 5% of Mn atoms, follow the shifts predicted for abundant Mn in Mouri and Enami. 40 On the other hand, the stronger nonlinear slope in most quadratic regression calibrations Fo#(f) (Table S2, Supplemental Material) introduces similar uncertainty to Fo samples, which are not compensated by the large set statistics that can be used in this Fo# range.

Scattering in the data at low Fo# < 50 Figure 5 is obviously caused both by a limited number of available Fa-like olivine samples, also due to a stronger impact in Fa samples from impurities, first of all by other divalent cations (Mn, Ca, and Ni). We note that deviations of the low- and high-frequency modes from the Fa "mean" for our Fa-end-member sample, having about 5% of Mn atoms, obey the shifts as predicted for abundant Mn in Mouri and Enami. 40 On the other hand, the stronger nonlinear slope in most quadratic regression calibrations Fo#(f) Table S2, Supplemental Material brings similar uncertainty to Fo samples, not compensated by large set statistics that can be used in this Fo# range.

Special attention should be paid to the sample temperature, which is strongly influenced by the absorbed laser power. Temperature gradients of f (T) up to 1.2 cm^{-1} per 100 K have been reported both at elevated temperatures 43 and toward cryogenic ones. 44 The heat, induced by the absorption of the intense laser emission, may not diffuse out of the measurement point in particles with dimensions in the order of the mean free path of thermal phonons in the medium. This can cause extended above the ambient temperature of the sample (a few hundred K are possible 45) and the frequency shifts of the Raman signal due to this. We assume that such shifts might be applicable to the results of the powdered samples.

It is clearly evident that some of the proposed calibrations have biases that could potentially be attributed to the shifts in the derived frequencies, which would point to issues related to the calibration of spectrometers: in dispersion and absolute wavelength. We note that such information is often omitted or incomplete in the studies, e.g., when describing only a "final" calibration step, such as adjusting the reference spectrum of a silicon crystal to a certain Stokes shift (usually around 520.5 cm^{-1}). The most complete information is given in Kuebler et al.,35 reporting on a calibration of the dispersion using the lines of a neon arc lamp with a final adjustment of

the Stokes spectra to the silicon reference line at 520.5 cm^{-1}. The “instrumental” bias has been specially addressed in some studies. Two different spectrometers were used to obtain the value for a discrepancy in the data in Kuebler et al.35 Differences between the frequencies of the modes instead of single-mode calibrations were proposed in Mouri and Enami. 40 Ishibashi et al. 10 proposed to eliminate the instrumental differences by using the difference values for Fo# and Stokes shifts with respect to the reference values (ΔFo#(f) = Fo#(f Ref) − Fo#(f) and Δf = f Ref − f), in their case a Fo end-member, believing that this approach can significantly reduce the error margin in the calibration of spectrally dispersive devices.

We checked the relevance and accuracy of different regressions Fo#(f) Table S2, Supplemental Material, based on the single band (linear, quadratic, differential linear, and differential quadratic) and based on both bands (ellipsoidal), using their absolute values, as well as when adjusted to the end-members, using only the small linear shift in the frequency (expressed in relative wavenumbers). The results of such fittings are shown in Figures 5b and 6.

The differential linear regressions I1 and I2, 10 which are supposed to be free of instrumental bias, were obtained for the limited Fo#62.8–100 range, and deviate from the “main line” (which can be considered as presented in “best ellipsoid” in Kuebler et al., 35 Figure 5 toward high-Fe olivines. Their extension to troctolite for the high frequency band gives a fairly good fit, apparently due to the small nonlinear contribution to the ΔFo#(f) slope Figure 5b.

The linear regressions for a single band (Ag(Si–O) s−str) or (A g(Si–O) a−str) show their inherent limitations in predicting Fo# in the entire range, 0–100 Figure 5. The regressions P1 and P2 fit the centroid of Fo# quite well. 41 For our samples, the P2 regression shows an excellent fit to the Fo and troctolite samples, slightly worse for the P1 regression, but it may not be accurate enough for the Fa endmembers.

The quadratic regressions for a single band show multidirectional proximity to the data sets at the low- and high-Fe content. Our data for the troctolite sample are in close vicinity to most quadratic regressions in general, i.e., not worse than for Fo, while the data for Fa are close to the “center of mass” of various approximations at low Fo#

Figure 5a. This leads to a tendency that the “absolute” calibrations, i.e., the calibration coefficients in the quadratic regression are taken as reported, and return better proximity to the EMPA data for the troctolite as those obtained by the adjusting of the regression to the end-members. The latter does not yield better accuracy overall, while adjusting to the Fa-sample generally yields worse results Figure 6.

This is also true for the nonlinear regression based on both bands (fa−st ; f s−st).35 This is very likely due to the large bias in the Raman line frequencies obtained for the Fa-

sample from the “optimal Fo#(f a−st); Fo#(f s−st) ellipsoid” 35 (as marked by the wide DB regressions in Figure 5.

Note that the frequency values for the Fo sample are well centered within the “optimal ellipsoid.” Furthermore, adjusting the regression towards the Fo-endmember does not improve the prediction for troctolite compared to the calibration that uses data for both endmembers (two-band calibration). However, the two-band calibration returns reasonable values within just a few units of the EMPA data for the troctolite sample.

Surprisingly, the differential quadratic regression 10 delivers almost worse results. We guess that this, in principle, the best approach to mitigating instrumental issues, suffers much from the limited input, i.e., the samples with high Fo#62.8–100. Obviously, the larger range of Fo# in a calibration set, extended toward the Fa-endmember, would be at least competitive with other absolute calibrations. On the other hand, the quadratic differential regression proposed by Mouri et al. 40 gives a good fit, although our data do not show good proximity to the single bands as noted in the cited study. The quadratic regression obtained by multivariant analysis of the largest set of samples and the data reported in the Raman database, 38 shows reasonable proximity for the mid- and high-Fo# and a larger deviation toward the Fa-endmember, which is clearly related to the density of input data on the different sides of Fo#.

The quadratic regressions adequately describe the ΔFo# (f) dependences and provide good predictions for the olivines between the end-members, either using the calibration as reported or as adjusted to the Fo#(f a−st); Fo#(f s−st) values of the (Fa, Fo)-end-members.

The obtained predicted Fo# for our troctolite sample (EMPA Fo#44.63) is based on the following:

Quadratic regression based on the single-band:

k 1: 40 absolute: 50.5 ± 0.9; to Fa-shifted 44.0 ± 0.8; to Fo-shifted: 33.2 ± 1.1.

OB1: 39 absolute: 39.5 ± 0.9; Fa-shifted: 43.5 ± 1.0; Fo-shifted: 42.4 ± 1.0.

DB2: 35 absolute: 50.5 ± 0.9; Fa-shifted: 44.3 ± 0.9; Fo-shifted: 39.5 ± 0.8.

Multivariate analysis (MVA): 38 absolute: 42.1 ± 0.2; Fa-shifted: 46.5 ± 0.2; Fo-shifted: 50.6 ± 0.2.

Quadratic regression based on both bands:

DB1 + DB2:35 absolute: 47.0 ± 1.0; Fa-shifted: 49.8 ± 1.0; Fo-shifted: 47.0 ± 1.0.

Quadratic differential regression based on the both bands: 39 46.9 ± 0.5.

Thus, the accuracy of #Fa within 3% can be provided by Raman spectroscopy analysis.

Among the quadratic regressions for the single band, Fo# (f a−st) or Fo#(fs−st), we choose: For the low-frequency band: those with the weakest quadratic slopes in the regressions:

> k 140 and OB1; 39 note that our three Fo# lie on the parabolic arc fit with the slightly larger quadratic slope (Table S2, Supplemental Material).

For the high-frequency band: those with the largest quadratic slopes in the regressions:

> DB2 35 and MVA; 38 our three Fo# lie on the parabolic arc fit between these quadratic slopes (Table S2, Supplemental Material).

Adjustment to the endmembers improves the derived values: toward the Fa-end-member for the low-frequency band f s−st and toward the Fo-end-member for the high frequency band fast . While a single, high-Fo# calibration sample may serve as a good estimate of the olivine composition, the regressions based on two bands, Fo#(f a−st) and Fo#(f s−st) bring a certain “stability” to the variations in the frequencies f a−st; fs−st. We note that regardless of the closeness of our data to the single-band fit, the differential fits, based on regressions to the band frequency difference, show a good fit for the troctolite sample. This indicates indirectly the importance of instrumental calibration for the absolute values of the pho non frequencies.

Laser-Induced Plasma Spectroscopy

All major elements in olivines exhibit sufficiently intense transitions of their neutral species (commonly used index (I) in the transition description, see Figure 7 and appear to be well detectable at relatively low laser intensities, just above laser ablation thresholds.

To calibrate the emission line intensity, used for quantitative estimates, we used the intensities of several Fe(I), Mg(I), and Mn(I) transitions, normalized to the intensity of a Si(I) transition at 288.2 nm of the same (individual) spectrum. The latter reduces the pulse-to-pulse irreproducibility of the plasma characteristics, the main uncertainty factor in LIBS analytics. The spectra of the Ol-endmembers indicate which transitions can be chosen for calibration, namely: presented in both LIBS spectra. The small number of these transitions indicates the need for calibration, since the so-called calibration-free LIBS analysis 46 cannot be applied with such limited inputs.

The abundance of Fe, Mg, and Mn in the samples is then based on a calibration of the end-members Fo and Fa.

Troctolite was calibrated due to the obtained EMPA values for the molar% of these elements Figure 8.

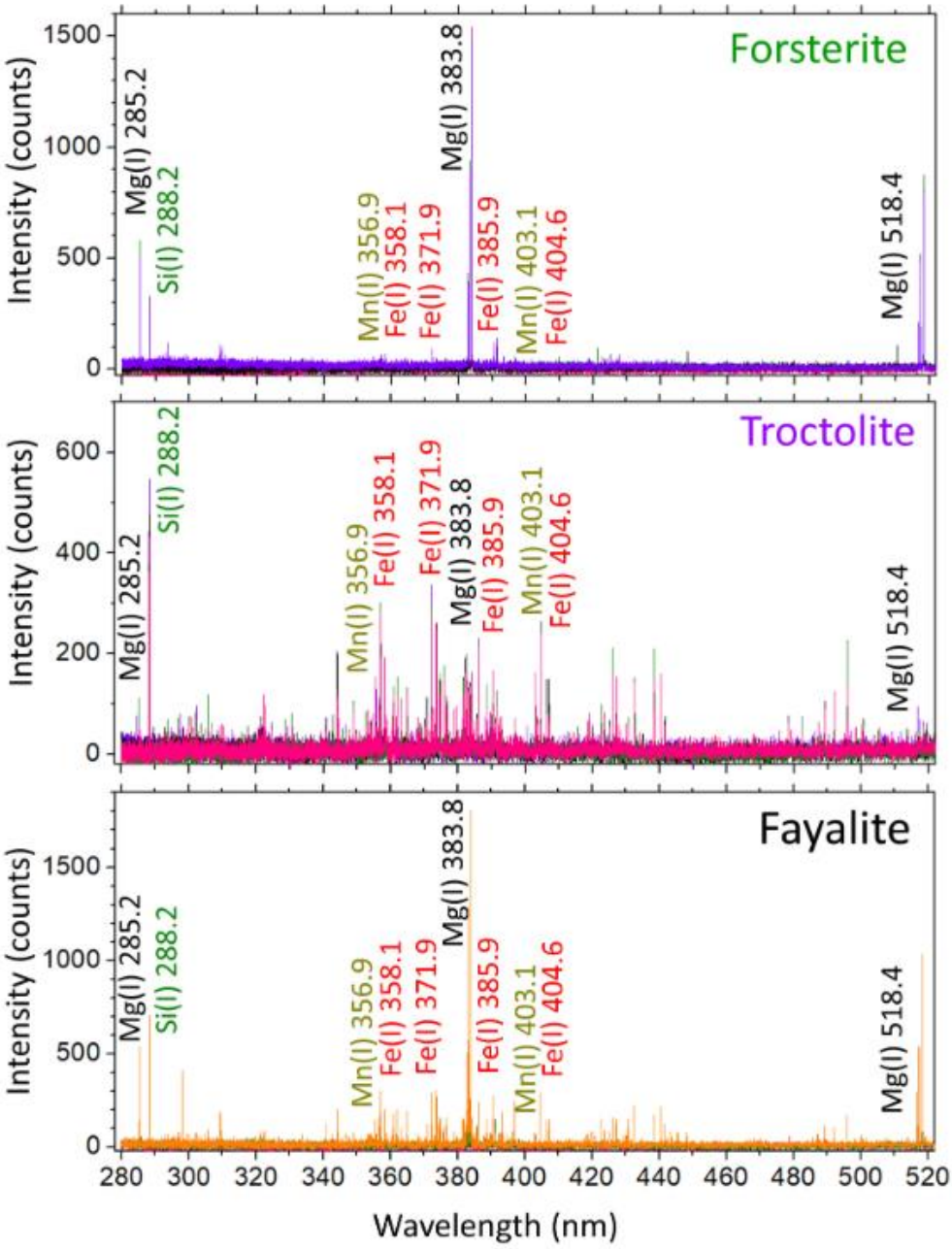

Figure 7. Laser-induced breakdown spectroscopy (LIBS) spectra recorded at different positions of the Fo, Tr, and Fa samples and displayed in the spectral range of the transitions used for calibration. These neutral atomic intracenter transitions of the elements are shown together with the transition wavelengths (in nm). For more detailed LIBS spectra with all assigned lines, see Supplemental Material.

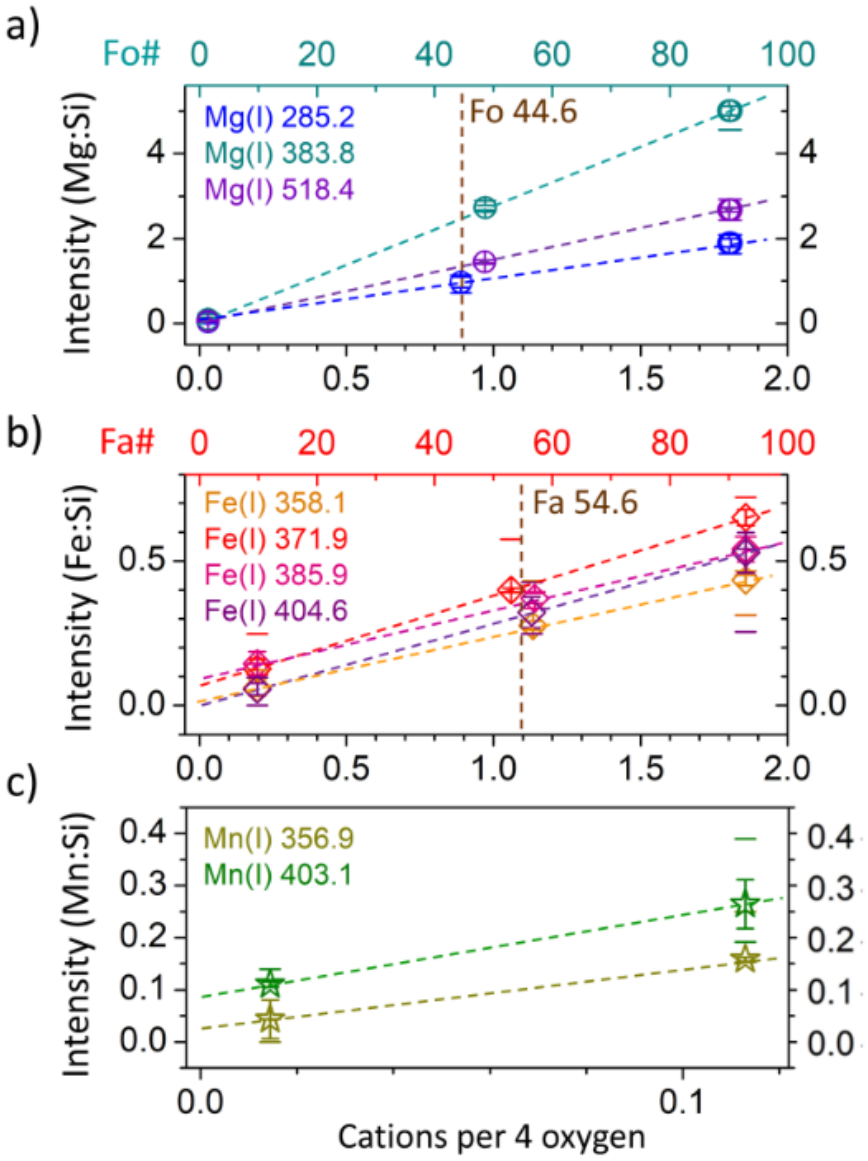

Figure 8. Calibration of the relative atomic abundances plotted as intensities of the transitions, normalized on a Si(I) 288.2 nm line, for the main cations, as presented in the LIBS spectra through the EMPA values for the reference Ol-end-members, given in the cations per four oxygen atoms. (a) Mg(I) lines, the upper axis in the Fo# units; (b) Fe(I) lines, the upper axis in the Fa# units; (c) Mn(I) lines for the Tr (lower Mn) and Fa (higher Mn) samples. Vertical dashed lines mark the Fo# or Fa# values for the troctolite sample according to EMPA analysis. Other dashed lines in (a) and (b) are linear fits to the reference Ol-end-members.

It is clear that the low-intense signals can lead to inaccurate outputs: for example, not all calibration curves for Mn and Fe transitions pass through the point (0;0) Figures 8b and 8c. Most Mg and Fe transitions yield calibrations that provide Fo# and Fa# values with reasonable scatter and closeness to the EMPA data for the troctolite sample.

The derived Fo# and Fa# values for the troctolite sample (the EMPA ' Mg#44.6; Fe#54.6) are as follows: from the calibration on the line Mg(I) 285.2 nm: Mg# 44.5 ± 3.8; Mg(I)

383.8 nm: Mg# 48.6 ± 1.8; Mg(I) 518.4 nm: Mg# 48.5 ± 1.5; Fe(I) 358.1 nm: Fe# 56.7 ± 3.2; Fe(I) 371.9 nm: Fe# 53.0 ± 1.2; Fe(I) 385.9 nm: Fe# 57.0 ± 3.1; Fe(I) 404.6 nm: Fe# 56.5 ± 7.9.

Despite a very small number of the acquired LIBS spectra, most of the strong and moderate transitions of Mg and Fe atoms can be used to calibrate olivine with a moderate tolerance, in the same order as the LIBS technique usually predicts for solid targets. The observed deviations of the calibration dependences from linear fit passing through zero and those derived for low intense signals are very likely due to nonvanishing nonlinear inputs, such as collisional and radiation resonant energy transfer to iron atoms. Such an effect could lead to positive biases in the LIBS responses. The influence of such contributions to the calibration curves decreases with increasing intensities of the calibrating transitions Figure 8a.

Despite the large uncertainty in the obtained values, the calibrations of Fo# and Fa# are close enough between the positions used and can be applied for reasonable estimates of the margins to the troctolite sample studied, providing Mg# with an accuracy of 5.8% for the mean and Fe# with an accuracy of 4.4% for the mean.

Conclusion

In general, all-optical spectroscopies considered provide estimates of the olivine composition in the complex rock sample (troctolite) with sufficient accuracy (below a few mol%), which would be a great return from such a limited calibration input and a limited number of acquired spectra. Even if one assumes different biases in an in situ experiment, one can expect good performance from these techniques. Raman scattering shows an excellent analytic output and has, in our opinion, a clear priority due to the available accurate calibrations of olivine, including those using differential Stokes shifts of two main vibrational modes, which additionally requires a proper calibration of the Raman spectrometer.

This involves accurate knowledge of the laser wavelength, which can be derived using the calibration target. A single calibration target on the Fo side might be sufficient for in situ calibration of the Raman spectrometer, however, the second calibration end-member provides a further step toward better accuracy. Quadratic regressions using the main vibrational bands provide more accurate values for the chemical composition of olivine.

Greater contrast in spectral features between chemically close mineral groups together with spectrally smooth/flat background signals make Raman spectroscopy advantageous over the IR reflectance technique. The high spatial resolution of Raman analytics leads to a very small optically accessed area and essentially no volume

interaction due to the inherent surface-type light-and-matter interaction. This makes Raman advantageous over LIBS, where the signal-to-noise ratio depends on the volume of ablated material. A single calibration target on the Fo side could be sufficient for in situ calibration of the Raman spectrometer.

The LIBS technique demonstrates good accuracy for olivine and also captures the abundance of those minor elements that can affect the cation side of complex olivine. This feature is missing in the Raman analysis of troctolite based on two stretching modes only. These additional cations can cause visible frequency shifts affecting the accuracy of the Raman analysis. Application of LIBS to complex rocks is known to encounter challenges in molecular analysis, which arise from the use of multi-variate techniques with statistical requirements that are often not satisfied in in situ scenarios with limited resources. Two calibration samples would significantly increase the accuracy of Fo# and Fa# determination by atomic emission spectroscopy.

Infrared (IR) reflectance has certain limitations for mineral composition analysis due to generally broader spectral bands (compared to Raman-active or atomic transitions, and also more pronounced in troctolite rock) and due to the strong dependence of the reflection band shapes on the relative orientation of microcrystals in the sample, a common scenario in the field. However, reflectance instruments in the thermal MIR (800–1100 cm^{-1}) require no excitation lasers, enabling lightweight, low-power, robust instruments at the expense of a modest reduction in accuracy. Since there are no issues related to the drift of (unnecessary) laser parameters, the wavelength calibration of IR instruments is based on the spectra acquired from calibration targets under sunlight irradiation.

Acknowledgments

The authors thank the Museum für Naturkunde in Berlin, Germany, and the Gilles Allard Collection, Museum of Natural History, University of Georgia, Athens, USA for supporting this study with dedicated samples.

Declaration of Conflicting Interests

The authors declared no potential conflicts of interest with respect to the research, authorship, and/or publication of this article.

Funding

The authors received no financial support for the research, authorship, and/or publication of this article.

Supplemental Materials

All supplemental material mentioned in the text is available in the online version of the journal.

References

1. J.A. Manrique, G. Lopez-Reyes, A. Cousin, F. Rull, et al. “SuperCam Calibration Targets: Design and Development”. Space Sci. Rev. 2020. 216(8): 138. 10.1007/s11214-020-00764-w

2. Y. Kawakatsu, K. Kuramoto, T. Usui, H. Sugahara, et al. “Preliminary Design of Martian Moons eXploration (MMX)”. Acta Astronaut. 2023. 202: 715–728. 10.1016/j.actaastro.2022.09.009

3. F.G.F. Gibb, J. Zussman. “Zoned Olivines in Four Apollo 12 Samples”. Earth Planet. Sci. Lett. 1971. 11(1–5): 161–167. 10.1016/0012-821X(71)90159-2

4. T.M. Hoefen, R.N. Clark, J.L. Bandfield, M.D. Smith, et al. “Discovery of Olivine in the Nili Fossae Region of Mars”. Science. 2003. 302(5645): 627–630. 10.1126/science.1089647

5. B.L. De Vries, B. Acke, J.A.D.L. Blommaert, C. Walekens, et al. “Comet-Like Mineralogy of Olivine Crystals in an Extrasolar Proto-Kuiper Belt”. Nature. 2012. 490(7418): 74–76. 10.1038/ nature11469

6. T. Nakamura, T. Noguchi, M. Tanaka, M.E. Zolensky, et al. “Itokawa Dust Particles: A Direct Link Between S-Type Asteroids and Ordinary Chondrites”. Science. 2011. 333

(6046): 1113–1116. 10.1126/science.1207758

7. M.E. Zolensky, T.J. Zega, H. Yano, S. Wirick, et al. “Mineralogy and Petrology of Comet 81p/Wild 2 Nucleus Samples”. Science. 2006. 314(5806): 1735–1739. 10.1126/science.1135842

8. J. Blundy, E. Melekhova, L. Ziberna, M.C.S. Humphreys, et al. “Effect of Redox on Fe–Mg–Mn Exchange Between Olivine and Melt and an Oxybarometer for Basalts”. Contrib. Mineral. Petrol. 2020. 175: 103. 10.1007/s00410-020-01736-7

9. I. Kushiro, M.J. Walter. “Mg-Fe Partitioning Between Olivine and Mafic-Ultramafic Melts”. Geophys. Res. Lett. 1998. 25(13): 2337–2340. 10.1029/98GL01844

10. H. Ishibashi, M. Arakawa, J. Yamamoto, H. Kagi. “Precise Determination of Mg/Fe Ratios Applicable to Terrestrial Olivine Samples Using Raman Spectroscopy”. J. Raman Spectrosc. 2012. 43(2): 331–337. 10.1002/jrs.3024

11. J.L. Bishop, J.F. Bell III, J.E. Moersch. Remote Compositional Analysis. Techniques for Understanding Spectroscopy, Mineralogy, and Geochemistry of Planetary Surfaces. Cambridge, UK: Cambridge University Press, 2020.

12. P.R. Christensen, M.B. Wyatt, T.D. Clotch, A.D. Rogers, et al. “Mineralogy at Meridiani Planum from the Mini-TES Experiment on the Opportunity Rover”. Science. 2004. 306 (5702): 1733–1739. 10.1126/science.1104909

13. M.D. Lane, P.R. Christensen. “Determining Olivine Composition of Basaltic Dunes in Gale Crater, Mars, from Orbit: Awaiting Ground Truth from Curiosity”. Geophys. Res. Lett. 2013. 40 (14): 3517–3521. 10.1002/grl.50621

14. J.W. Salisbury. “Mid-Infrared Spectroscopy: Laboratory Data”. In: C.M. Pieters, P.A.J. Englert, editors. Remote Geochemical Analysis: Elemental and Mineralogical Composition. Cambridge, UK: Cambridge University Press, 1993. Chap. 4. Pp. 79–98.

15. F. Rull, S. Maurice, I. Hutchinson, A.G. Moral, et al. “The Raman Laser Spectrometer for the ExoMars Rover Mission to Mars”. Astrobiology. 2017. 17(6–7): 627–654. 10.1089/ast.2016.1567

16. R. Bhartia, L.W. Beegle, L. DeFlores, W. Abbey, et al. “Perseverance’s Scanning Habitable Environments with Raman and Luminescence for Organics and Chemicals (SHERLOC) Investigation”. Space Sci. Rev. 2021. 217: 58. 10.1007/ s11214-021-00812-z

17. Y. Cho, U. Böttger, F. Rull, H.-W. Hübers, et al. “In Situ Science on Phobos with the Raman Spectrometer for MMX (RAX): Preliminary Design and Feasibility of Raman Measurements”. Earth Planets Space. 2021. 73: 232. 10.1186/s40623-021-01496-z

18. R.C. Wiens, S. Maurice, B. Barraclough, M. Saccoccio, et al. “The ChemCam Instrument Suite on the Mars Science Laboratory (MSL) Rover: Body Unit and Combined System Tests”. Space Sci. Rev. 2012. 170: 167–227. 10.1007/s11214-012-9902-4

19. S. Maurice, R.C. Wiens, P. Bernardi, P. Cais, et al. “The SuperCam Instrument Suite on the Mars 2020 Rover: Science Objectives and Mast-Unit Description”. Space Sci. Rev. 2021. 217: 47. 10.1007/s11214-021-00807-w

20. A.S. Laxmiprasad, R.V.L.N. Sridhar, A. Goswami, K.A. Lohar, et al. “Laser Induced Breakdown Spectroscope on Chandrayaan-2 Rover: A Miniaturized Mid-UV to Visible Active Spectrometer for Lunar Surface Chemistry Studies”. Current Science. 2020. 118(4): 573–581.

21. J.W. Salisbury, L.S. Walter, N. Vergo, D.M. D’Aria. “Infrared (2.1–25 μm) Spectra of Minerals”. https://pubs.usgs.gov/of/ 1987/0263/report.pdf [accessed Nov 20 2024].

22. Z. Ren, M. Guo, Y. Cheng, Y. Wang, et al. “A Review of the Development and Application of Space Miniature Mass Spectrometers”. Vacuum. 2018. 155: 108–117. 10.1016/j. vacuum.2018.05.048

23. National Institute of Standards and Technology (NIST). “Energy Level of Neutral Iron (Fe I)”. https://physics.nist.gov/PhysRefData/ Handbook/Tables/irontable5_a.htm [accessed Feb 2 2024].

24. A.M. Hofmeister. “Single-Crystal Absorption and Reflection Infrared Spectroscopy of Forsterite and Fayalite”. Phys. Chem. Miner. 1987. 14: 499–513. 10.1007/BF00308285

25. A.M. Hofmeister. “Infrared Reflectance Spectra of Fayalite, and Absorption Data from Assorted Olivines, Including Pressure and Isotope Effects”. Phys. Chem. Min. 1997. 24: 535–546. 10.1007/s002690050069

26. A.M. Hofmeister, K.M. Pitman. “Evidence for Kinks in Structural and Thermodynamic Properties Across the Forsterite–Fayalite Binary from Thin-Film IR Absorption Spectra”. Phys. Chem. Miner. 2007. 34: 319–333. 10.1007/s00269-007-0150-1

27. M.D. Lane, T.D. Glotch, M.D. Dyar, C.M. Pieters, et al. “Midinfrared Spectroscopy of Synthetic Olivines: Thermal Emission, Specular and Diffuse Reflectance, and Attenuated Total Reflectance Studies of Forsterite to Fayalite”. J. Geophys. Res. 2011. 116(E8): E08010. 10.1029/2010JE003588

28. Y. Zhu, Y. Li, H. Ding, A. Lu, et al. “Vibrational and Structural Insight into Silicate Minerals by Mid-Infrared Absorption and Emission Spectroscopies”. Phys. Chem. Minerals. 2022. 49: 6. 10.1007/s00269-022-01180-y

29. V.E. Hamilton. “Thermal Infrared (Vibrational) Spectroscopy of Mg–Fe Olivines: A Review and Applications to Determining the Composition of Planetary Surfaces”. Geochemistry. 2010. 70(1): 7–33. 10.1016/j.chemer.2009.12.005

30. C.H. Kremer, J.F. Mustard, C.M. Pieters. “Cross-Over Infrared Spectroscopy: A New Tool for the Remote Determination of Olivine Composition”. Geophys. Res. Lett. 2020. 47(20): e2020GL089151. 10.1029/2020GL089151

31. S.V. Gaisler, B.A. Kolesov. “Raman Spectra of Olivine Solid Solutions (FexMg 1−x)2 SiO4 and Spin-Vibration Interaction”. J. Struct. Chem. 2007. 48: 61–65. 10.1007/s10947-007-0009-9

32. A. Bischoff. “Meteorite Classification and the Definition of New Chondrite Classes as a Result of Successful Meteorite Search in Hot and Cold Deserts”. Planet. Space Sci. 2001. 49(8): 769–776. 10.1016/S0032-0633(01)00026-5

33. R.N. Clark, G.A. Swayze, R.A. Wise, K.E. Livo, et al. “USGS Digital Spectral Library Splib06a”. https://pubs.usgs.gov/ publication/ds231 [accessed November 20 2024].

34. A. Chopelas. “Single Crystal Raman Spectra of Forsterite, Fayalite, and Monticellite”. Am. Mineral. 1991. 76(7–8): 1101–1109.

35. K.E. Kuebler, B.L. Jolliff, A. Wang, L.A. Haskin. “Extracting Olivine (Fo–Fa) Compositions from Raman Spectral Peak Positions”. Geochim. Cosmochim. Acta 2006. 70(24): 6201–6222. 10.1016/j.gca.2006.07.035

36. B.L. do Nascimento-Dias, T.P. Donato, M.E. Zucolotto, V. deCarvalho dos Anjos. “Raman Spectral Peak Positions of Olivine (Fo–Fa) as Fast Methodology for Classifying Chondrites”. J. Raman Spectrosc. 2021. 52(6): 1206–1211.10.1002/jrs.6114

37. RRUFF Project. “RRUFF Database of Raman Spectra, X-ray Diffraction, and Chemistry Data for Minerals”. https://rruff. info/ [accessed Feb 2 2024].

38. L.B. Breitenfeld, M.D. Dyar, C.J. Carey, T.J. Tague Jr, et al. “Predicting Olivine Composition Using Raman Spectroscopy Through Band Shift and Multivariate Analyses”. Am. Mineral. 2018. 103(11): 1827–1836. 10.2138/am-2018-6291

39. I. Torre-Fdez, C. García-Florentino, J. Huidobro, L. Coloma, et al. “Characterization of Olivines and Their Metallic Composition: Raman Spectroscopy Could Provide an Accurate Solution for the Active and Future Mars Missions”. J. Raman Spectrosc. 2023. 54(3): 340–350. 10.1002/jrs.6485

40. T. Mouri, M. Enami. “Raman Spectroscopic Study of Olivine-Group Minerals”. J. Mineral. Petrol. Sci. 2008. 103(2): 100–104. 10.2465/jmps.071015

41. L. Pittarello, K. Baert, V. Debaille, P. Claeys. “Screening and Classification of Ordinary Chondrites by Raman Spectroscopy”. Meteorit. Planet. Sci. 2015. 50(19): 1718–1732. 10.1111/maps.12506

42. B.A. Kolesov, J.V. Tanskaya. “Raman Spectra and Cation Distribution in the Lattice of Olivines”. Mater. Res. Bull. 1996. 31(8): 1035–1044. 10.1016/S0025-5408(96)00085-2

43. B. Kolesov, C. Geiger. “A Raman Spectroscopic Study of Fe–Mg Olivines”. Phys. Chem. Minerals 2004. 31: 142–154. 10.1007/s00269-003-0370-y

44. I. Weber, U. Böttger, S.G. Pavlov, E.K. Jessberger, H.-W. Hübers. “Mineralogical and Raman Spectroscopy Studies of Natural Olivines Exposed to Different Planetary Environments”. Planet. Space Sci. 2014. 104(Part B): 163–172. 10.1016/j.pss.2014.08.016

45. U. Böttger, S.G. Pavlov, N. Deßmann, F. Hanke, et al. “Laser-Induced Alteration of Raman Spectra for Micron-Sized Solid Particles”. Planet. Space Sci. 2017. 138: 25–32. 10.1016/j. pss.2017.02.001

46. N. Zhang, T. Ou, M. Wang, Z. Lin, et al. “A Brief Review of Calibration-Free Laser-Induced Breakdown Spectroscopy”. Front. Phys. 2022. 10: 887171. 10.3389/fphy.2022.887171